ARTICLE

Predicting the resistance profile of a spudcan penetrating sand overlying clay

Pan Hu, Dong Wang, Mark J. Cassidy, and Sam A. Stanier

Abstract: Assessment of the risk of punch-through failure of spudcan foundations on sand overlying clay requires prediction of the full penetration resistance profile, from touchdown and through punch-through to equilibrium of the vertical resistance at depth in the underlying clay layer. This study uses the Coupled Eulerian–Lagrangian approach, a large deformation finite element analysis method, to model the complete penetration resistance profile of a spudcan on sand overlying clay. The sand is modeled using the Mohr–Coulomb model, while the clay is modeled using a modified Tresca model to account for strain softening. The numerical method is then used to simulate a series of spudcan penetration tests, performed in a geotechnical centrifuge, on medium dense sand overlying clay. The punch-through behavior observed in the experiments is replicated, and the penetration resistance profiles from numerical analyses are generally a reasonable match to the experimental measurements. The influences of the sand layer height to foundation diameter ratio, sand–clay interface shear strength, and strength gradient in clay on the penetration resistance profiles are explored in a complementary parametric study. The penetration resistance in the underlying clay layer is well predicted using a simple linear expression for the bearing capacity factor for the spudcan and underlying sand plug. This expression is combined with an existing failure stress dependent model for predicting peak resistance to form a simplified method for prediction of the full penetration resistance profile. This new method provides estimates of the vertical penetration that the spudcan will run during the punch-through event. It is validated against both medium dense and dense sand centrifuge tests.

Key words: spudcan, sand, clay, punch-through, centrifuge modeling, finite element method.

Résumé : L'évaluation du risque de rupture en perforation de fondations de type caisson de support sur de l'argile couverte de sable nécessite la prédiction du profil complet de résistance à la pénétration, de la mise en place au sol à la perforation et jusqu'à l'équilibre de la résistance verticale en profondeur dans la couche d'argile sous-jacente. Cette étude utilise l'approche Eulérienne-Lagrangienne couplée, une méthode d'analyse par éléments finis à grande déformation, pour modéliser le profil complet de résistance à la pénétration d'un caisson de support sur de l'argile couverte de sable. Le sable est modélisé à l'aide du modèle Mohr-Coulomb, tandis que l'argile est modélisée à l'aide d'un modèle Tresca modifié pour considérer l'adoucissement des déformations. Le modèle numérique est ensuite utilisé pour simuler une série d'essais de pénétration de caissons de support, réalisés dans une centrifugeuse géotechnique, sur de l'argile couverte de sable moyen dense. Le comportement en perforation observé dans les essais est répliqué, et les profils de résistance à la pénétration obtenus par les analyses numériques correspondent généralement bien avec les mesures expérimentales. Les influences du ratio de la hauteur de la couche de sable par rapport au diamètre de la fondation, de la résistance au cisaillement de l'interface sable-argile et du gradient de résistance dans l'argile sur la résistance à la pénétration sont explorées grâce à une étude paramétrique complémentaire. La résistance à la pénétration dans la couche d'argile inférieure est bien prédite à l'aide d'une expression linéaire simple du facteur de capacité portante pour le caisson de support et le bouchon de sable sous-jacent. L'expression est combinée avec un modèle existant de rupture dépendante de la contrainte servant à prédire la résistance au pic afin de former une méthode simplifiée pour la prédiction du profil complet de résistance à la pénétration. Cette nouvelle méthode donne des estimations de la pénétration verticale que le caisson de support subira durant les évènements de perforation. Elle est validée avec des essais en centrifugeuse sur des sables moyens denses et sur des sables denses. [Traduit par la Rédaction]

Mots-clés : caisson de support, sable, argile, perforation, modélisation par centrifugeuse, méthode par éléments finis.

Introduction

The unexpectedly sudden and rapid penetrations of spudcan foundations during installation are a major risk to the stability of jack-up platforms. This can occur when under vertical loading the large (often ~20 m diameter) spudcan pushes a layer of strong sandy material into an underlying weak clay layer. Rapid spudcan and leg penetration occurs until the applied jack-up weight (and preloading ballast weight) equates with the resistance in the underlying clay layer. If not handled properly, the large displace-

ment of the leg may cause damage to the structure of the jack-up or down time. This type of event is termed a punch-through failure.

To assess the risk of punch-through during the installation of jack-up rigs, an accurate prediction of the spudcan penetration resistance profile is critical. Two "wished-in-place" methods are recommended by the ISO (2012) guidelines to estimate the peak penetration resistance of a spudcan in layered strata where punch-throughs might be a possibility. In both methods, the bearing capacity is calculated at a specified penetration depth, assuming

a pre-embedded spudcan and undisturbed soil stratigraphy and strengths. When used to back-calculate centrifuge data, the ISO (2012) prediction methods significantly underestimate the potential for punch-through (Hu et al. 2014). There are currently no guidelines for the calculation of the bearing capacity following punch-through into the underlying clay layer that account for the combined bearing capacity of the spudcan and any sand trapped beneath, as observed by Teh et al. (2008) using particle image velocimetry (PIV) analysis.

Simple methods are needed to predict the full penetration resistance profile for a spudcan penetrating through sand overlying clay that can be used routinely in site-specific assessment of jack-up safety (Osborne et al. 2006). Such methods should account for the mechanistic changes that occur at different stages of penetration, as observed by Teh et al. (2008). For simplicity, two key events might be used to define the severity of a punch-through event: (*i*) the magnitude and depth of peak resistance in the sand layer, and (*ii*) the depth at which the resistance in the underlying clay layer becomes equal to the peak resistance. The depth between these two events is thus an estimate of the plunge depth that may be experienced in the field during preloading and can be used to check against serviceability limits for the jack-up platform. For the measurement of plunge depth from the testing profile, a tangent line from the depth at which the spigot is fully embedded following the penetration resistance profile towards peak resistance is constructed, followed by a vertical line to the equilibrium depth in the clay layer (where the current resistance is equal to the peak resistance in sand). The depth of the punch-through event, d_{punch}, is the length of the line from the depth of peak resistance until vertical equilibrium is re-established.

The magnitude and depth of the peak resistance in the sand layer is readily calculable using the failure stress dependent method derived by Lee et al. (2013*b*) for dense sand overlying clay. This model assumes that an inverted and truncated cone of sand is pushed down into the underlying clay, mobilizing shearing around the periphery of the inverted truncated cone and clay bearing capacity at the base. Stress dependent dilatancy is incorporated into the model using a modified form of Bolton's correlations by relating the dilatancy to the bearing pressure at failure (Bolton, 1986). The form of this model was enhanced by Hu et al. (2014) to account for the mobilization embedment depth and further validated experimentally for medium dense to dense sand states.

Calculating the bearing capacity in the underlying clay is complicated by sand trapped underneath the spudcan. The bearing capacity of a spudcan in clay is commonly expressed as

$$(1) \qquad q_{\text{clay}} = N_c s_{u0} + \frac{V_f \gamma_c'}{A}$$

where N_c is the bearing capacity factor; s_{u0} is the intact soil strength at the lowest elevation of the spudcan widest cross-sectional area (termed the load reference point (LRP)); V_f is the embedded foundation volume below the spudcan LRP; γ_c' is the effective unit weight of the clay; A is the nominal surface area of the foundation ($A = \pi D^2/4$, where D is the diameter of the spudcan). The first term is the bearing capacity for a weightless soil, while the second term accounts for buoyancy. Following punch-through on sand overlying clay, the bearing capacity factor N_c and volume of the foundation V_f should be related to the composite geometry of the foundation and the trapped sand plug. However, the application of eq. (1) is difficult for this scenario due to uncertainty about the trapped sand plug volume and geometry. For example, Teh et al. (2008) observed using PIV analyses that the upper portion of the trapped sand beneath the spudcan resembled a cylinder with diameter similar to the spudcan, whereas the shape of the lower part was slightly irregular due to the meta-

stable state of the trapped sand. In the experiments of Teh et al. (2008), the trapped sand plug height, H_{plug}, was ~$1H_s$, where H_s is the height of the sand layer. Lee (2009) performed a series of small strain numerical analyses that assumed that the spudcan and sand plug could be idealized as a composite cylindrical foundation. Expressions for N_c were related to the assumed composite foundation height and diameter, facilitating prediction of the full penetration resistance profile from a measured soil shear strength profile. In contrast to Teh et al. (2008), Lee (2009) found that a range of H_{plug} of $0.6H_s$ to $0.9H_s$ was required to attain a good fit to the experimental measurements. Such uncertainty limits confidence in the application of eq. (1) and further verification is necessary. An alternative approach is to back-calculate the bearing capacity factors from the experimental measurements of full spudcan load penetration tests, as performed by Lee et al. (2013*a*), resulting in

$$(2) \qquad N_c = 14\frac{H_s}{D} + 9.5 \quad \left(0.21 \le \frac{H_s}{D} \le 1.12\right)$$

The full penetration resistance profile can also be predicted using large deformation finite element methods. These methods require no prior assumption of the failure mechanisms and may be used in conjunction with advanced constitutive models to attempt to faithfully replicate soil behavior. Compared with traditional Lagrangian finite element methods, large deformation analysis avoids severe mesh distortion. Two such methods have been used to replicate the continuous penetration process of a spudcan on sand overlying clay-

1. The remeshing and interpolation technique with small strain-RITSS method was used by Yu et al. (2012) to investigate the effects of the undrained shear strength of the underlying clay and the thickness and friction angle of the upper sand. A simple equation was proposed to relate the post-peak bearing capacity factor to the soil properties in which the bearing capacity factor is directly related to the strength ratio between the sand and the clay

$$(3) \qquad N_c = 3.3\left(\frac{H_s \gamma_s' \tan\phi'}{s_{u0}}\right) + 12$$

where γ_s' and ϕ' are the effective unit weight and internal friction angle of sand, respectively. However, this equation is summarized based on a limited numerical study and does not account for the increase of N_c with H_s/D observed experimentally by Lee et al. (2013*a*).

2. The coupled Eulerian–Lagrangian (CEL) approach that is available in the commercial package ABAQUS/Explicit. The CEL approach was first adopted for research on spudcan performance by Tho et al. (2009, 2012) to compare numerical penetration resistances and soil flow mechanisms with centrifuge results. Qiu and Henke (2011) and Qiu and Grabe (2012) later incorporated hypoplastic and visco-hypoplastic constitutive models into the CEL approach to better simulate the complex rate and strain hardening-softening dependent behaviors of sand and clay. No recommendations on the bearing capacity factor for the composite spudcan and sand plug in the underlying clay were provided in previous CEL studies.

In this paper, the CEL approach is used to simulate continuous spudcan penetration on loose and medium dense sand overlying clay with increasing shear strength with depth, while accounting for strain softening in the clay layer. The numerical methods are first validated by comparison with previous numerical and centrifuge test data for spudcan penetration in normally consolidated clay and in uniform sand. The impacts of mesh density, penetra-

tion rate, foundation interface friction, and clay softening are then considered. The CEL analyses are conducted to simulate a series of centrifuge tests performed on medium dense sand overlying clay alongside a parametric study that broadens the scope to cover the geometric conditions relevant to spudcan punch-through in the field. Sand plug heights and bearing capacity factors in the clay layer are then inferred from the CEL analyses and are shown to be a good fit for a simple linear relationship. These simple equations can be used to predict the bearing capacity profile in the lower clay layer and, when coupled with the failure stress-dependent model by Hu et al. (2014), to derive an estimate for the depth of a punch-through event. The performance of the simplified prediction method is verified against experimental centrifuge data for medium dense to dense sand overlying clay.

Numerical methodology

Implementation of CEL approach

In the CEL approach, the spudcan and soil are discretized using Lagrangian and Eulerian mesh, respectively. The Eulerian mesh is composed of 8-node linear hexahedron elements with reduced integration and hourglass control. The soil materials are allowed to flow through Eulerian elements whose nodes have fixed locations (Dassault Systèmes 2011). The Eulerian mesh is initially composed of two parts, one that is initially occupied by soil and another that is void to accommodate any soil heave created during the penetration process. An Eulerian element may be partially void or filled with multiple materials. The presence and volume fractions of different materials in each Eulerian element are specified at the beginning of the analysis. In contrast, only one material is contained in a Lagrangian element. During the analysis, the Eulerian material is tracked as it flows through the mesh by computing its volume fraction within each element.

Each incremental step in a CEL analysis consists of two phases, Lagrangian and Eulerian. An updated Lagrangian calculation is conducted in an explicit integration scheme, followed by an Eulerian phase in which advection is performed to map the solution variables (such as material properties, stresses, strains, velocities, and accelerations) from the deformed mesh to the original mesh. The Eulerian material boundaries and interfaces are updated through the volume fractions of each material and generally do not correspond to element boundaries.

The contact interactions between different Eulerian materials (sand and clay) were not defined because the materials deform continuously, and there is no slip between them. The interaction between the Eulerian materials (soils) and the Lagrangian material (spudcan) was described with a "general contact" algorithm that is based on frictional contact using the penalty method. Rather than the traditional small sliding frictional formulation, a finite sliding formulation was implemented to consider arbitrary slide on the interface in large deformation problems. During spudcan penetration into sand overlying clay, contact between the spudcan and sand will be maintained during the entire penetration process. Frictional interaction between the spudcan and sand was defined through a roughness factor (Cassidy and Houlsby 2002)

$$(4) \qquad \alpha = \frac{\tan\delta}{\tan\phi'}$$

where δ is the interface friction angle between the sand and spudcan.

The current CEL approach in ABAQUS/Explicit has only three-dimensional elements. By taking advantage of geometrical symmetry, only one quarter of the spudcan and soil were modeled. The geostatic stresses due to the submerged unit weight of the soil were imposed before spudcan penetration, with a coefficient of

lateral earth pressure of $(1 - \sin\phi')$ for the sand layer and unity for the clay layer.

To enhance the solution accuracy, the soil region in contact with the spudcan must be refined. The penetration of a spudcan was simulated with displacement control. In contrast, spudcan penetration in the field is a load-controlled quasi-static process; hence, the penetration rate adopted in the CEL simulations, which is based on an explicit integration scheme, needs to be sufficiently low to avoid inertial effects. In the penetration resistance profiles presented herein, the depth of penetration, d, was zero when the LRP contacts the soil.

Constitutive models

The spudcan penetration rates in practical offshore applications are on the order of 1–3 m/h. Penetration rates in centrifuge model tests are usually selected such that drained deformation occurs in the upper sand layer, while undrained response occurs in the clay layer (Teh et al. 2010; Lee et al. 2013a; Hu et al. 2014). This arrangement is achieved by specifying that the normalized velocity vD/c_v (where v is the absolute penetration rate and c_v is the coefficient of consolidation) is in the range of 30–300 for the clay layer and less than 0.01 for the sand layer (Finnie and Randolph 1994; Low et al. 2008; Cassidy 2012).

Loose to medium dense sand usually shows a hardening rather than softening response under drained conditions, so the sand layer was modeled as an elastic – perfectly plastic material with a Mohr–Coulomb yield criterion. The internal frictional angle was specified as the critical value, unless otherwise stated, because (i) the primary aim is to model the deep penetration resistance in the clay layer following punch-through; (ii) the sand beneath the advancing spudcan undergoes extremely large deformation, and (iii) it has been shown by Li et al. (2013) to reach the critical state during deep penetration (in the clay layer). The sand volume is stable at the critical state; therefore, the dilation angle was $\psi = 0$.

The clay layer under undrained conditions was modeled as an elastic – perfectly plastic material with the Tresca yield criterion. The Poisson's ratio was 0.49 to approximate constant volume under undrained conditions. Because soil rigidity only slightly affects the penetration resistance, a typical Young's modulus of $500s_u$ was used throughout, where s_u is the current undrained shear strength of the clay considering softening. The effect of strain softening is incorporated following Einav and Randolph (2005) by modifying the shear strengths at the integration points according to the accumulated absolute plastic shear strain

$$(5) \qquad s_u = \left[\delta_{rem} + (1 - \delta_{rem})e^{-3\xi/\xi_{95}}\right]s_{ui}$$

where s_{ui} is the intact undrained shear strength; δ_{rem} denotes the ratio of fully remolded and initial shear strengths (the inverse of the sensitivity, S_t); ξ is the accumulated absolute plastic shear strain; and ξ_{95} represents the value of ξ required for the soil to undergo 95% remolding, estimated in the range of 10 to 50 for marine clays. In CEL implementations, the plastic shear strain increments in the clay layer were recorded to update the soil strength at the integration point through eq. (5), and the updated strength was approximated as constant during the calculations of the subsequent step.

The chosen shear strength profile was based on that measured in the centrifuge tests. The intact undrained strength profile was measured using a T-bar penetrometer and was found to increase linearly with soil depth

$$(6) \qquad s_{ui} = s_{um} + kz$$

where s_{um} is the clay strength at mudline for a single clay layer or at the sand–clay interface for sand overlying clay, k is the strength gradient, and z represents the soil depth. Hossain and Randolph

Fig. 1. (*a*) Numerical and analytical analyses for spudcan penetration into normally consolidated clay; (*b*) deformed clay strength profile at penetration depth of 3*D*.

(*a*) (*b*)
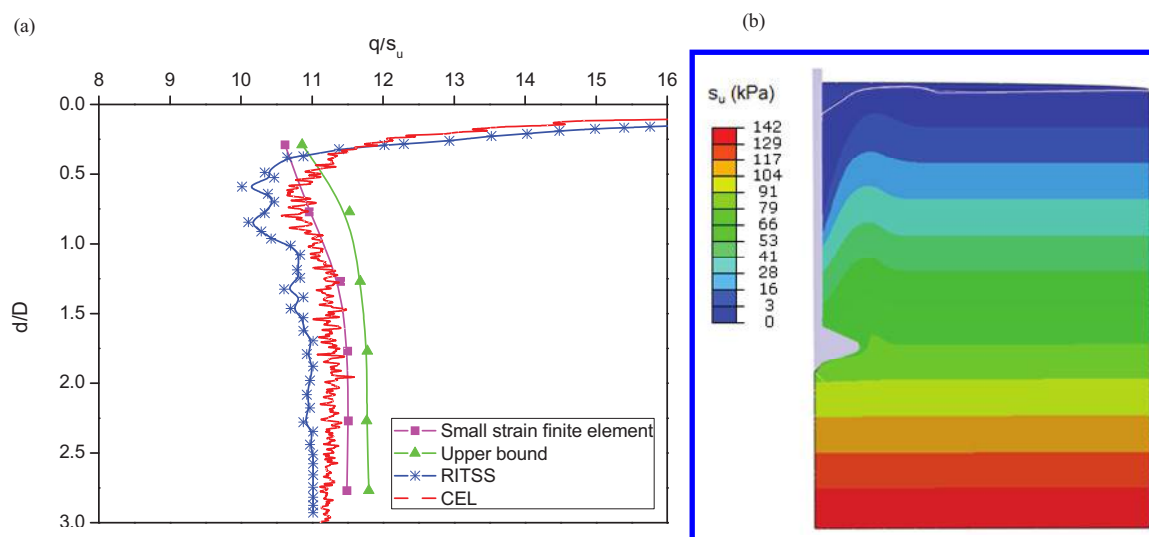
(2009) found that the average shear strain rates induced in soils by spudcan and t-bar penetrometers were comparable; hence, it was unnecessary to consider the potential for shear strength enhancement due to rate effects.

Verification of the CEL approach

Spudcan penetration in a single clay layer

The bearing capacity factor of spudcan in normally consolidated clay has been investigated using different analytical and numerical approaches. A spudcan with a diameter of 14 m penetrating in normally consolidated clay was studied by Mehryar and Hu (2002) using the RITSS approach. Detailed spudcan dimensions can be found in Fig. 1 in Mehryar and Hu (2002). The submerged unit weight of clay, γ'_c, was 7 kN/m³, the undrained shear strength was $s_{ui} = 2z$ kPa, and no strain softening was considered. A CEL simulation was performed for comparison, with a penetration rate of 0.25 m/s, which was sufficiently slow to generate a quasi-static response. The typical element size around the spudcan was 0.036*D*. The bearing capacity factors from the CEL, RITSS, traditional small-strain finite element (FE), and plasticity limit analyses are presented in Fig. 1*a*. In the latter two analyses, the spudcan was assumed to be pre-embedded at different depths because the continuous penetration process cannot be tracked. As *d*/*D* > 0.5, the bearing capacity factor predicted by the CEL is slightly higher than that predicted by the RITSS method; however, the bearing capacity factors from both approaches converge to ~11 at *d*/*D* of 3. The bearing capacity factors obtained from both large deformation finite element (LDFE) approaches are moderately lower than that of the wished-in-place spudcans; the bearing capacity is overestimated if the drag-down of weaker soil indicated in Fig. 1*b* is ignored. The soil radially within ~1*D* of the centerline of the spudcan is significantly disturbed by the penetration process.

### Spudcan penetration in a single sand layer

White et al. (2008) reported a centrifuge test of a conical footing (very similar to a spudcan) with a diameter of 4.8 m on medium dense sand (relative density $I_D = 54\%$). A CEL simulation was performed, assuming a Poisson's ratio of 0.3 and Young's modulus of 50 MPa. A constant *m* in correlations by Bolton (1986) was fitted by back-calculation as 0.85 by White et al. (2008), while *m* is typically 3 for a triaxial stress state. Corresponding operative friction angles calculated using Bolton's correlations were 33.22° and 36.32° for these two scenarios, so an average value of 34.8° was assumed

Fig. 2. Comparison of CEL with a centrifuge test for spudcan penetration into medium dense sand.
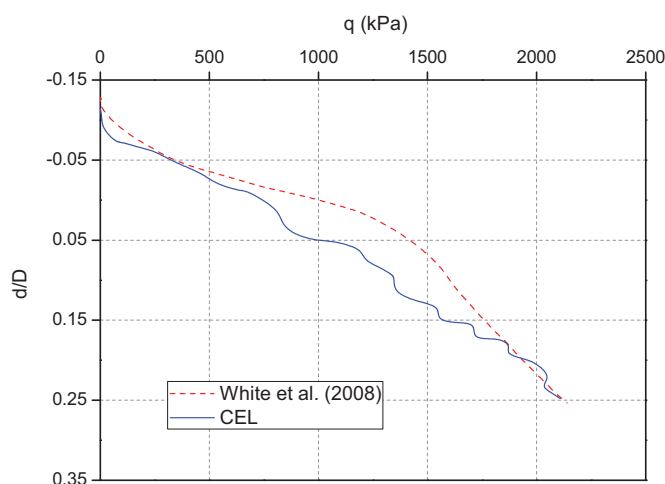
in the current analysis, along with a dilation angle of $\psi = 4.8°$ that was similarly based on Bolton's correlations. A friction coefficient of $\alpha = 0.5$ on the spudcan–sand interface was adopted (the influence of which will be discussed in the "Effects of spudcan roughness and S_t on penetration resistances" section). The penetration rate was 0.1 m/s, and the element size around the spudcan was ~0.03*D*. The footing geometry in the CEL analysis was identical to the model used in the centrifuge tests.

As shown in Fig. 2, the numerical bearing capacity shows a trend similar to the experimental data with a maximum difference of ~20%. The difference may be due to the constant soil properties assumed in the CEL simulation. During the very early stages of penetration, the friction angle of the sand in reality is likely to be moderately higher than the value used in the CEL analyses because the friction angle in the numerical analyses did not vary with mean stress level. The friction angle may reduce gradually to a nearly constant value with increasing capacity during further penetration, which is consistent with the behavior modeled in the CEL analysis. For the spudcan penetration in loose or medium dense sand overlying clay, the simple and robust Mohr–Coulomb model was deemed adequate, as the primary concern was capturing the volume, geometry, and bearing capacity

Fig. 3. Nomenclature for spudcan foundation penetration in sand overlying clay.
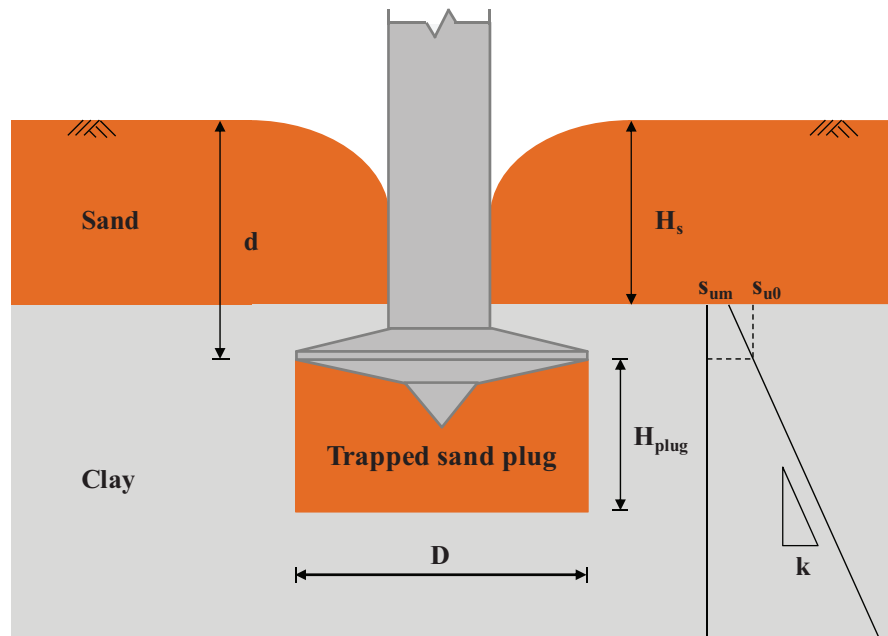
Fig. 4. Prototype dimensions of spudcan model (Note: dimensions are absolute values, and spigot tip to shoulder heights vary with D).
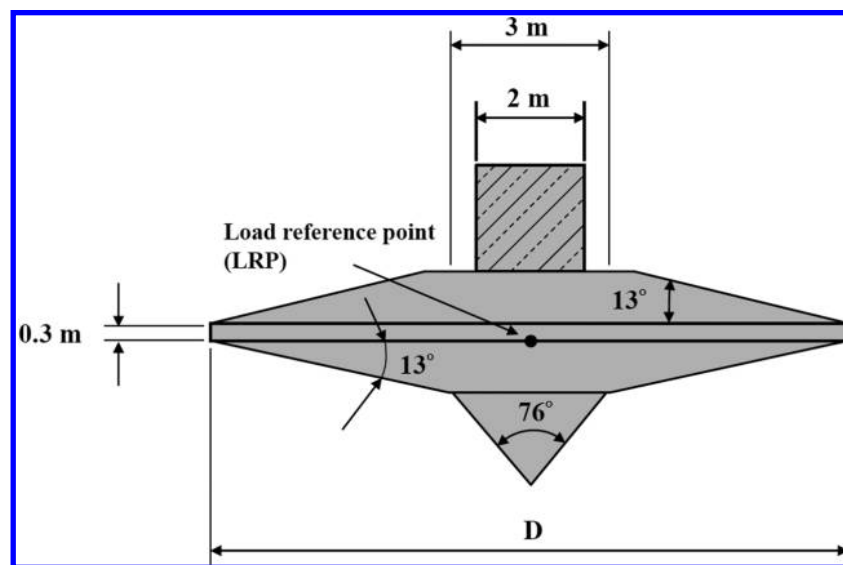
characteristics in the clay layer of the composite foundation comprising the spudcan and sand plug. The periphery of the sand plug is expected to be subjected to large shear strains during penetration and thus will likely be at the critical state. Therefore, the adoption of the Mohr–Coulomb model with a friction angle equal to the critical value is considered appropriate.

Simulation of centrifuge tests of medium dense sand overlying clay

The penetration of a spudcan in medium dense sand overlying clay (see nomenclature in Fig. 3) behaves differently from that in a single clay or sand layer. CEL simulations were performed to replicate a total of 15 centrifuge tests (relative density $I_D = 43\%$) by Hu et al. (2014). The spudcan model of the centrifuge tests (Fig. 4), with a 13° shallow conical underside profile and 76° protruding spigot, was simulated for direct comparison with the experiments. The spudcan diameters and soil properties of each test are listed in Table 1. The Poisson's ratio and Young's modulus of sand were assumed to be 0.3 and 25 MPa, respectively. The critical state friction angle was 31° for the super fine sand used in the centrifuge test (White et al. 2008). The sensitivity of the underlying kaolin clay, S_t, was 3, based on cyclic t-bar measurements.

A typical test, L1SP1, with $D = 6$ m and normalized sand thickness $H_s/D = 1$, was used as an example to demonstrate the mesh convergence, penetration rate for quasi-static simulation, and effects of spudcan roughness and sensitivity of clay on penetration resistance.

Mesh convergence and penetration rate

Mesh convergence studies were conducted to ensure that the Eulerian mesh was sufficiently fine to avoid overestimation of the penetration resistance. Four typical element sizes, indicated as a ratio of the spudcan diameter, were adopted close to the spudcan: 0.018D, 0.025D, 0.03D, and 0.05D. The meshes had corresponding numbers of soil elements of 490821, 220031, 142560, and 49197,

Table 1. Prototype parameters and results of centrifuge and numerical tests of medium dense sand and dense sand overlying clay.

Experimental details								Results						
	Geometry			Sand		Clay		Test			CEL			
Test name	H_s (m)	D (m)	H_s/D	I_D (%)	γ'_s (kN/m³)	s_{um} (kPa)	k (kPa/m)	q_{peak} (kPa)	H_{plug} (m)	d_{punch} (m)	q_{peak} (kPa)	H_{plug} (m)	$N_{c, deep}$	Prediction method: d_{punch} (m)
L1SP1	6	6	1	43	9.96	12.96	1.54	382.95	5.49	7.80	410.96	5.29	23.06	7.08
L1SP2	6	8	0.75	43	9.96	12.96	1.54	339.53	5.60	8.40	334.44	5.48	19.05	7.11
L1SP3	6	10	0.6	43	9.96	12.96	1.54	364.78	4.88	7.40	309.12	5.94	18.25	7.15
L1SP4	6	12	0.5	43	9.96	12.96	1.54	294.41	5.68	8.00	279.95	6.11	15.83	7.18
L1SP5	6	14	0.43	43	9.96	12.96	1.54	302.53	5.07	8.00	300.00	5.11	15.20	7.21
L2SP1	5	6	0.83	43	9.96	12.36	1.54	340.57	4.97	6.80	326.32	4.55	21.40	5.90
L2SP2	5	10	0.5	43	9.96	12.36	1.54	244.44	4.63	6.40	256.76	4.27	16.57	5.96
L2SP3	5	14	0.36	43	9.96	12.36	1.54	222.11	4.62	7.00	219.06	4.12	14.16	6.10
L2SP4	5	16	0.31	43	9.96	12.36	1.54	221.33	4.80	6.20	217.28	4.33	13.08	6.24
L2SP5	5	20	0.25	43	9.96	12.36	1.54	223.99	4.17	6.40	220.00	4.48	12.72	6.28
L3SP1	3.2	6	0.53	43	9.96	11.01	1.55	230.22	2.59	5.60	225.13	2.92	16.62	3.86
L3SP2	3.2	8	0.4	43	9.96	11.01	1.55	206.75	2.66	4.90	189.67	3.17	15.27	3.90
L3SP3	3.2	12	0.27	43	9.96	11.01	1.55	183.61	2.90	5.00	175.33	2.57	13.10	4.16
L3SP4	3.2	16	0.2	43	9.96	11.01	1.55	184.32	3.18	4.70	155.56	2.61	12.11	4.15
L3SP5	3.2	20	0.16	43	9.96	11.01	1.55	169.92	3.40	4.60	165.00	3.25	11.45	4.25
D1SP40a*	6.2	8	0.78	92	10.99	17.7	2	603	N/A	11.80	N/A	N/A	N/A	9.59
D1SP50a*	6.2	10	0.62	92	10.99	17.7	2	534	N/A	9.20	N/A	N/A	N/A	9.43
D1SP60a*	6.2	12	0.52	92	10.99	17.7	2	501	N/A	11.20	N/A	N/A	N/A	9.35
D1SP70a*	6.2	14	0.44	92	10.99	17.7	2	424	N/A	9.40	N/A	N/A	N/A	9.29
D1SP80a*	6.2	16	0.39	92	10.99	17.7	2	456	N/A	9.25	N/A	N/A	N/A	9.21

*Dense sand spudcan test from Lee (2009).

respectively. To minimize the computational cost, only a quarter of the domain was modeled. The mesh with element size of 0.025D is shown in Fig. 5. The spudcan was displaced at a penetration rate of 0.2 m/s. The penetration resistance profiles for the different mesh densities are shown in Fig. 6a. For an element size of 0.05D, the penetration resistance was overestimated significantly. In contrast, load displacement responses based on element sizes of 0.018D and 0.025D converged, suggesting that mesh convergence is achieved with an element size of 0.025D.

The penetration rate specified to result in a quasi-static analysis must be sufficiently slow; however, the computational cost increases with reduced penetration rate (Tho et al. 2012). The penetration resistance profiles for different penetration rates of 0.1, 0.2, 0.5, and 1 m/s are shown in Fig. 6b. The profiles corresponding to the penetration rates of 0.1 and 0.2 m/s show divergence of less than 2%. When the spudcan diameter is larger than 6 m, the inertial effect will become increasingly negligible.

Based on these sensitivity analyses, an element size close to the spudcan of 0.025D and a spudcan penetration rate of 0.2 m/s were selected for the remainder of the analyses. These parameters balance computational accuracy and efficiency.

Effects of spudcan roughness and S_t on penetration resistances

The effect of spudcan roughness on penetration resistance depends on the soil type. For a rough spudcan in a single clay layer, the penetration resistance is only ~5% higher than that of a smooth spudcan. In contrast, the roughness of a spudcan has a distinct influence on the penetration resistance in a single sand layer. Qiu and Henke (2011) conducted CEL simulations of spudcan penetration on a single sand layer and found that the penetration resistance was enhanced significantly when the friction coefficient α was increased from 0 to 0.5, but only increased by up to a further ~5% at deep penetrations for $\alpha > 0.5$.

The numerical penetration resistance profiles for sand overlying clay with α of 0, 0.5, and 1 are shown in Fig. 7. Overall, the resistance profile with α of 0.5 is close to that with α of 1. The penetration resistance in the clay layer with $\alpha = 0$ is significantly lower than those with $\alpha = 0.5$ and 1, with the divergence becoming increasingly apparent with increasing penetration depth (with a

Fig. 5. Typical finite element mesh used in CEL analysis.
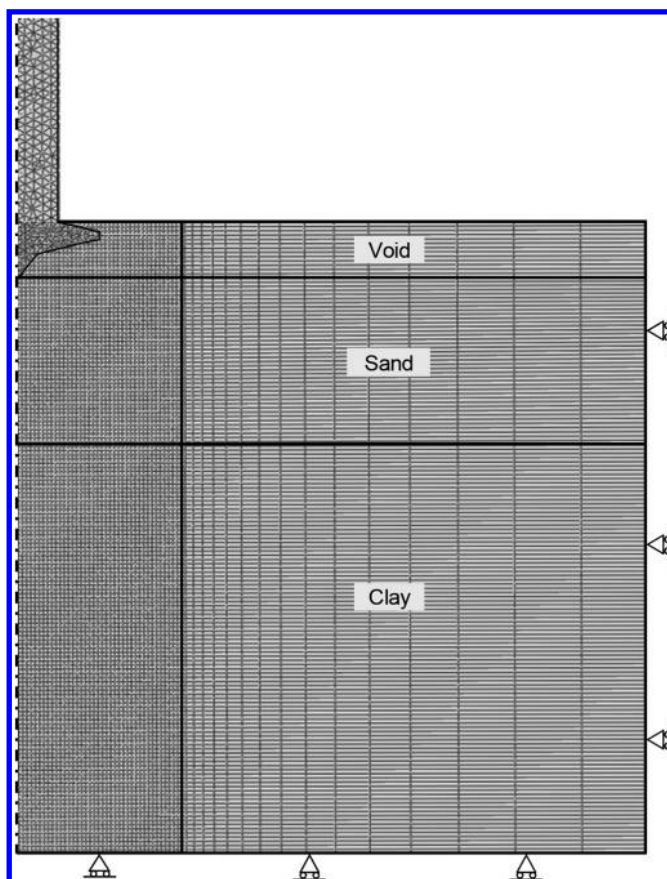
maximum difference of 22% at $d/D = 2.3$). The peak penetration resistance, q_{peak}, which appears in the sand layer, is almost independent of the spudcan roughness. The peak penetration resistance of a smooth spudcan ($\alpha = 0$) appears marginally higher than

Fig. 6. (*a*) Effects of mesh density; (*b*) effect of penetration rate.
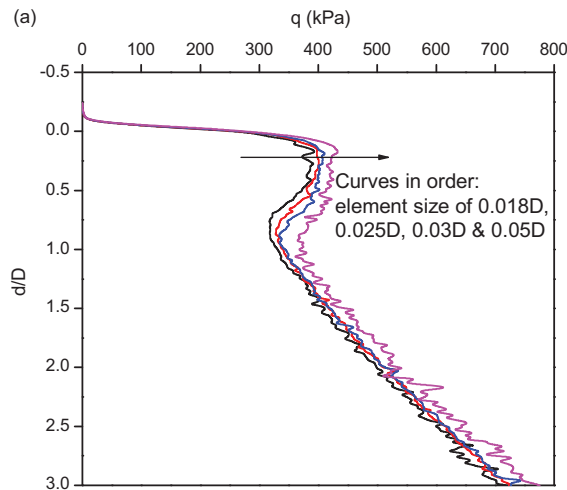
Fig. 7. Penetration resistance profiles for different contact properties.
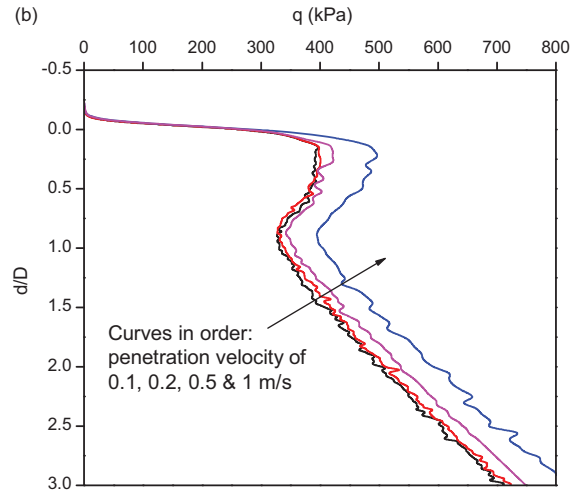
Fig. 8. Effect of soil sensitivity on penetration resistance profiles.
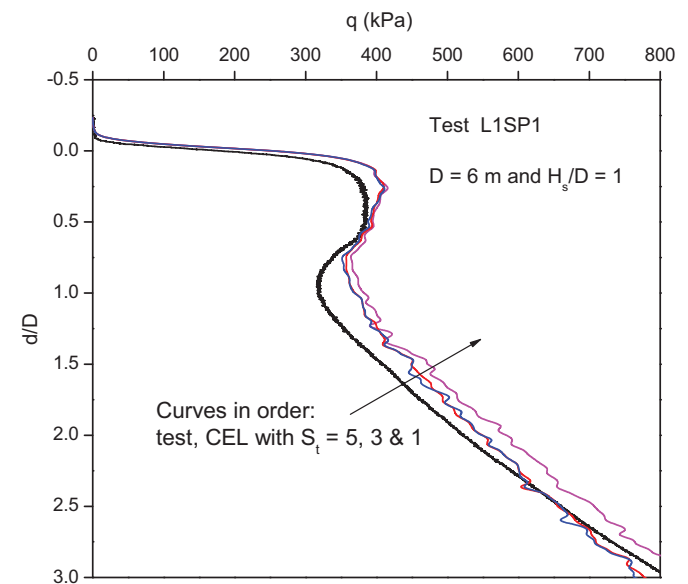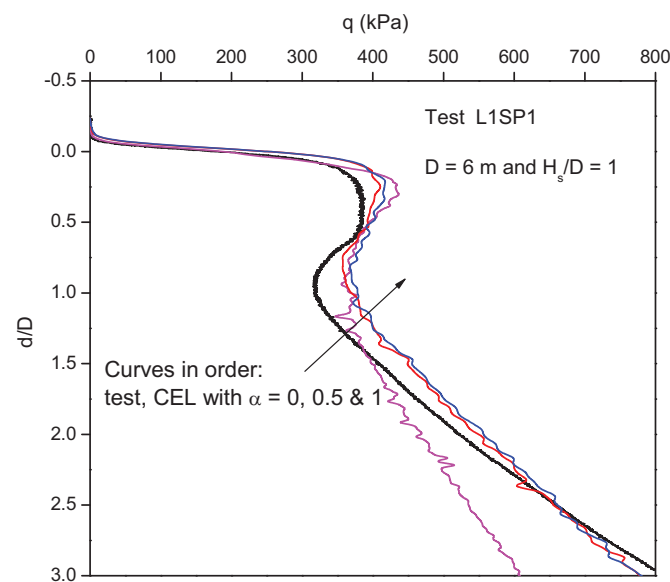
those of intermediate or fully rough spudcans. The potential cause of this difference is the greater amount of soil flow in the sand layer leading to more strength mobilization in the layer, while for the rough spudcan such mobilization is not obvious and the failure mechanism concentrates mainly at the layer interface. When the spudcan is penetrated into the clay layer, stronger sand is trapped beneath the advancing spudcan, and the shape and volume of the sand plug depends on the roughness of the spudcan. Compared with the smooth spudcan, more sand is trapped beneath the frictional spudcan, and the sand plug transfers the loading to deeper soil with higher local undrained strength. A roughness of $\alpha = 0.5$ was used in the following analyses to capture this effect.

Another potential concern in these simulations is that the shaft is treated as frictional like the spudcan to faithfully simulate the experiments of Hu et al. (2014), where the vertical load was measured at the top of the shaft. The impact of this detail was considered by performing an additional analysis for the smallest (6 m diameter) spudcan (for which the impact of friction on the shaft is largest given the same shaft was used for all spudcan sizes). In this analysis, the spudcan was assumed frictional with $\alpha = 0.5$, while

the shaft was frictionless. At a penetration depth of $H_s + D$ (a depth relevant to the interpretation of bearing capacity factors in the underlying clay layer presented later), the penetration resistance was reduced by no more than 7% for the frictionless shaft analyses compared to the frictional shaft counterpart. This result indicates that the impact of friction on the shaft was minimal.

For most offshore soft to medium soft clays, the typical range of soil sensitivity is S_t of 2–5 (Kvalstad et al. 2001; Andersen and Jostad 2004). The sensitivity of kaolin clay in centrifuge tests was measured by Hu et al. (2014) as $S_t = 3$, which is close to the S_t value of 2.5 by Zhang et al. (2011) and S_t of 2–2.5 by Gan et al. (2012) for the same soil. The penetration resistance profiles for $S_t = 1$, 3, and 5 are shown in Fig. 8. The profiles with $S_t = 3$ and 5 are nearly identical, while the penetration resistance is increased by 9% when the sensitivity is reduced from 3 to 1. A sensitivity of 3 is adopted in the following analyses for consistency with the experimentally measured sensitivity.

Full penetration resistance profiles

All 15 centrifuge tests reported by Hu et al. (2014) were grouped with three sand layer thicknesses: H_s of 3.2, 5, and 6 m. Two typical experimental penetration resistances for each sand layer height

Fig. 9. Penetration resistance profiles from centrifuge tests and CEL analyses: sand thickness of (*a*) 6 m, (*b*) 5 m, and (*c*) 3.2 m.
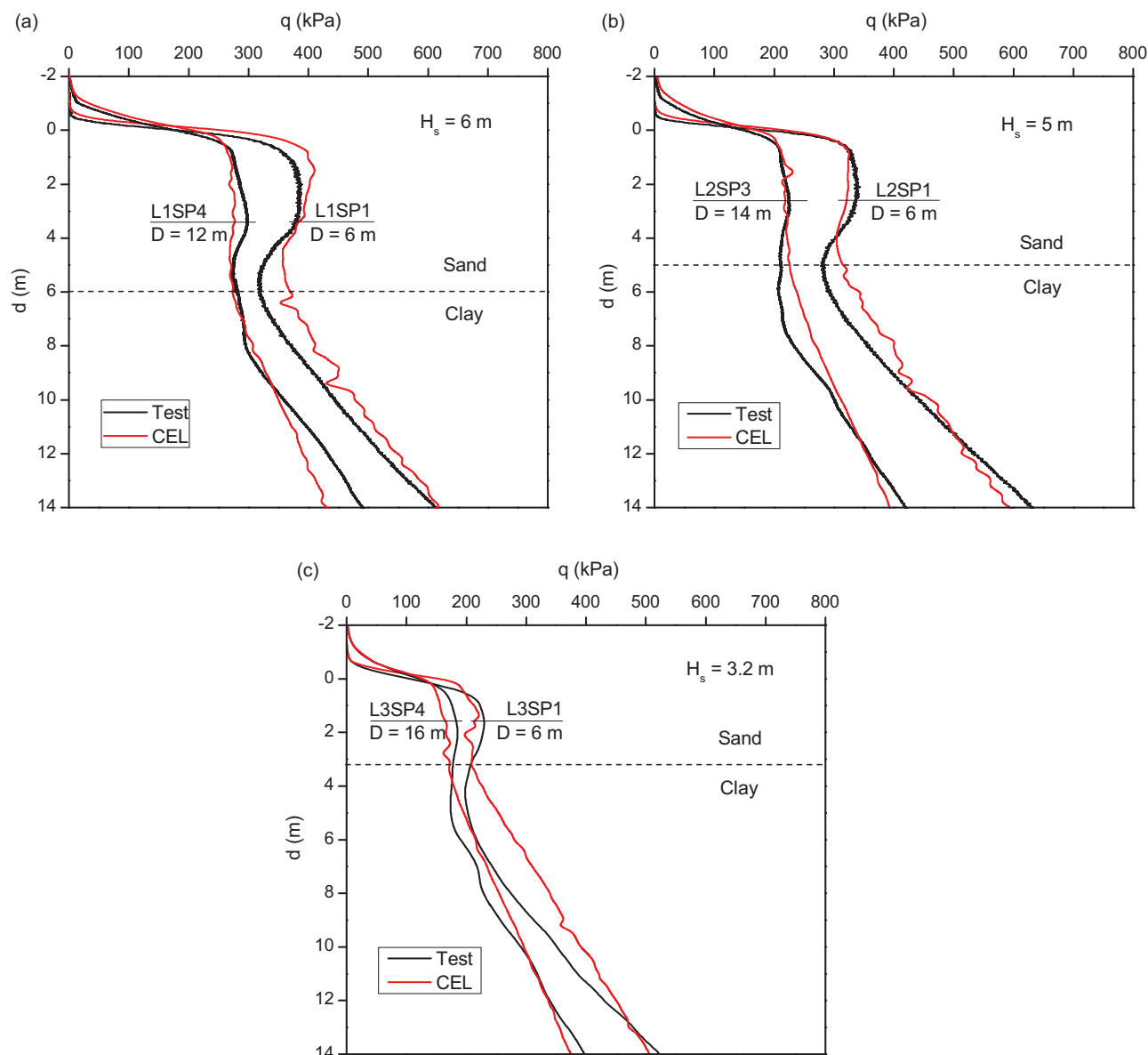
and corresponding numerical simulations are plotted in Fig. 9. Reasonable agreement is broadly evident between the CEL results and experiments. From touchdown of the tip of the spudcan to full embedment into the sand surface, the penetration resistance increases insignificantly, and soil flow is constrained within the sand layer. After the LRP touches the sand, the penetration resistance begins to be rapidly mobilized up to the peak resistance, q_{peak}, at a penetration depth of 0–2 m in the sand layer. The magnitude of q_{peak} depends on both the sand and clay strengths because, at this point, the sand frustum beneath the spudcan is being pushed into the underlying clay layer. The penetration resistance remains approximately constant or reduces slightly until the LRP of the spudcan penetrates into the underlying clay layer. The punch-through mechanisms observed in the centrifuge tests are generally captured by the simulations, despite the resistances in clay layer being overestimated for some cases. Following penetration of the spudcan and sand plug into the clay layer, the penetration resistance tends to increase proportionally with depth, which is mainly attributed to the linear increase in clay strength with depth. This result suggests that the shape of the composite

spudcan and sand plug foundation is essentially stable; thus, the bearing capacity factor may remain constant with depth.

Peak resistance and sand plug height

The peak resistance and corresponding penetration depth must be quantified in routine designs. The peak resistances measured in the centrifuge tests and predicted by the CEL approach and a modified failure stress-dependent model (Hu et al. 2014, and summarized in the section titled "Simplified method for prediction of full penetration resistance profile" of this paper) are compared in Fig. 10. The predictions from the numerical analyses and analytical model are in reasonable agreement within bounds of ±15%. The CEL analyses generally slightly under-predict the experimental peak resistance due to the assumption in the CEL analyses that the friction angle of sand is equal to the critical value. The analytical model calculations for the same experiments indicate transient operative friction angles slightly higher, 33°–34° at peak resistance. The critical friction angle was used here to appropriately model the shape and volume of the trapped sand plug where

Fig. 10. Peak penetration resistances from centrifuge tests, CEL analyses and predicted formulations.
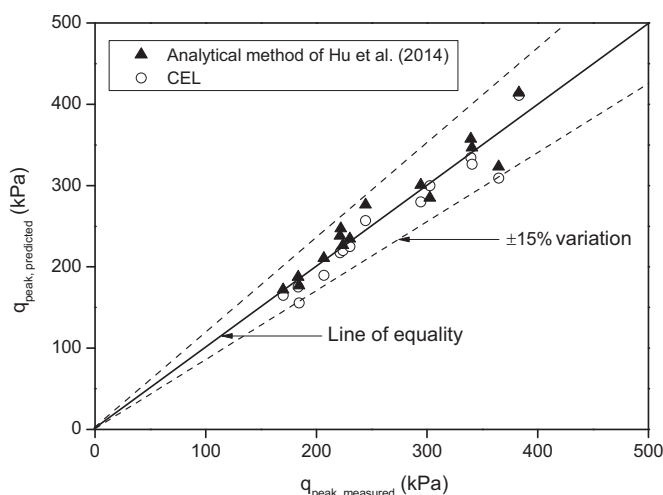
the sand at the periphery would be at the critical state (Li et al. 2013).

During penetration in the clay layer, the height of the sand plug, H_{plug}, is important, as it influences the bearing capacity factor and the buoyancy term of eq. (1). H_{plug} is a function of soil properties, spudcan diameter, and test geometry. For the centrifuge experiments described by Hu et al. (2014), all test locations were dissected to examine the deposited height of the trapped sand plug left in the clay after spudcan extraction. Typical sand plug geometries from tests L1SP1 and L1SP4 and the corresponding CEL simulations are presented in Fig. 11. All the sand plug heights H_{plug} inferred from the numerical simulations are close to those determined in the post test measurements illustrated in Fig. 12a, while Fig. 12b shows that both the experimental and CEL analyses resulted, on average, in trapped sand plug heights that were 90% of the sand layer thickness. This result is close to the value of $\sim 1H_s$ observed by Teh et al. (2008) and agrees with the upper bound estimated by Lee (2009). The bearing capacity in the clay layer, accounting for buoyancy, can thus be expressed as

$$(7) \qquad q_{clay} = N_c s_{u0} + H_{plug}\gamma'_c$$

$$= N_c s_{u0} + 0.9 H_s \gamma'_c \quad \left(\text{for } 0.16 \leq \frac{H_s}{D} \leq 1\right)$$

Parametric studies

Influences of sand thickness and undrained strength of clay

Before predicting the full penetration resistance profile, the influences of several critical factors (H_s/D, s_{um}, and k) were quantified within realistic bounds relative to offshore practices. A complementary set of parametric analyses were thus performed in addition to the experimental simulations, the geometric and soil property details of which are listed in Table 2. The sand thickness ratio H_s/D was varied from 0.3 to 0.9; clay strength at the sand-clay interface s_{um} from 10 to 40 kPa; clay shear strength gradient k from 1 to 2 kPa/m; and operative friction angle ϕ' from 30° to 33° (representative of typical critical friction angles for siliceous sands). The spudcan geometry (Fig. 4) was identical to that used in the experiments reported by Hu et al. (2014).

The normalized sand thickness, H_s/D, has an obvious influence on the penetration resistance, as shown in Fig. 13a. A punch-through potential is observed at $H_s/D = 0.7$, with a reduction in penetration resistance predicted during the vertical penetration. An approximately constant peak penetration resistance over the penetration depth is observed in the case of $H_s/D = 0.6$. In the

jack-up industry this is often referred to as a rapid-leg-run event. For smaller sand thicknesses, such as $H_s/D = 0.3$, safe installation is possible. This trend is due to the magnitudes of the sources of resistance that comprise q_{peak}. For larger H_s/D, shearing in the sand layer provides a far larger proportion of q_{peak} than the bearing capacity of the underlying clay layer. In contrast, for small H_s/D, the clay bearing capacity is dominant and provides the majority of q_{peak}. The clay bearing capacity is mainly dependent upon s_{um} and k, which do not change between these analyses; thus, catastrophic punch-through failure is more likely to occur with a higher H_s/D, as the difference between peak and post peak resistance is greatest. Figure 13a also shows that, for different sand thickness ratios, the penetration resistances in the clay layer do not converge due to the differing volume and geometry of the trapped sand plugs beneath the spudcan.

The effects of clay shear strength at the sand-clay interface, s_{um}, and strength gradient k on the penetration resistance are demonstrated in Fig. 13b, with $H_s/D = 0.6$. Rapid-leg-run potential is observed in all cases, and the depths of peak penetration resistance are nearly independent of the undrained strength of clay; however, the deep penetration resistance in the clay layer increases significantly with increasing s_{um} or k. For $k = 2$ kPa/m, $H_s/D = 0.6$, and $\phi' = 32°$, the peak resistance for s_{um} of 20 kPa is a factor of ~ 1.3 times that for s_{um} of 10 kPa. After the LRP reaches the original sand–clay interface, the gradient of the penetration resistance profiles is nearly independent of s_{um}, while the increasing rate of penetration resistance is larger for higher k after the spudcan is fully embedded in the clay layer. These trends are further indication that, for a constant geometric ratio H_s/D, a constant N_c should be used.

Equation for bearing capacity factor

When the spudcan and the sand plug penetrate into clay together, the sand plug mobilizes soil with a higher soil strength than that at the LRP due to the shear strength of the soil increasing with depth. Thus, the bearing capacity factors for spudcan penetration into a single clay layer are inappropriate for the sand overlying clay scenario investigated here.

The bearing capacity factor N_c was derived by dividing the bearing pressure by the intact undrained shear strength adopted in both the simulations of the centrifuge tests and the complementary parametric analyses. Both s_{u0} and N_c refers to the values at LRP in Fig. 4. When the LRP was penetrated to a depth deeper than $1D$ below the sand–clay interface (i.e., $(d - H_s)/D \geq 1$), it is observed that the spudcan with the sand plug underneath has reached a deep 'steady state' according to the CEL simulations of all centrifuge tests and complementary parametric studies. The capacity factor at $1D$ below the sand–clay interface can be fitted linearly against the sand thickness

$$(8) \qquad N_{c,deep} = 15\frac{H_s}{D} + 9 \quad \left(\text{for } 0.16 \leq \frac{H_s}{D} \leq 1\right)$$

with a coefficient of determination of $R^2 = 0.93$. This deep factor remains constant with further penetration in clay.

If the capacity factor at depth of $(d - H_s)/D < 1$ is approximated with eq. (8) (i.e., $N_c = N_{c,deep}$ from the depth of the sand–clay interface), the capacity factor is very close to the relationship given in eq. (2) that was fitted against the centrifuge tests for dense sand overlying clay (Lee et al. 2013a). Figure 14 demonstrates the normalized N_c profiles from the sand–clay interface to a depth of $2D$ below the sand–clay interface. In this figure, the capacity factor near the sand–clay interface ($d = H_s$) tends to be higher than $N_{c,deep}$. This is due to the trapped sand plug not being fully formed, causing some extra sand to shear close to the sand–clay layer interface. However, the typical depth at the end of punch-through events, as demonstrated below, is deeper than the depths

**Fig. 11.** Typical deformed sand and clay layers and sand plug heights.
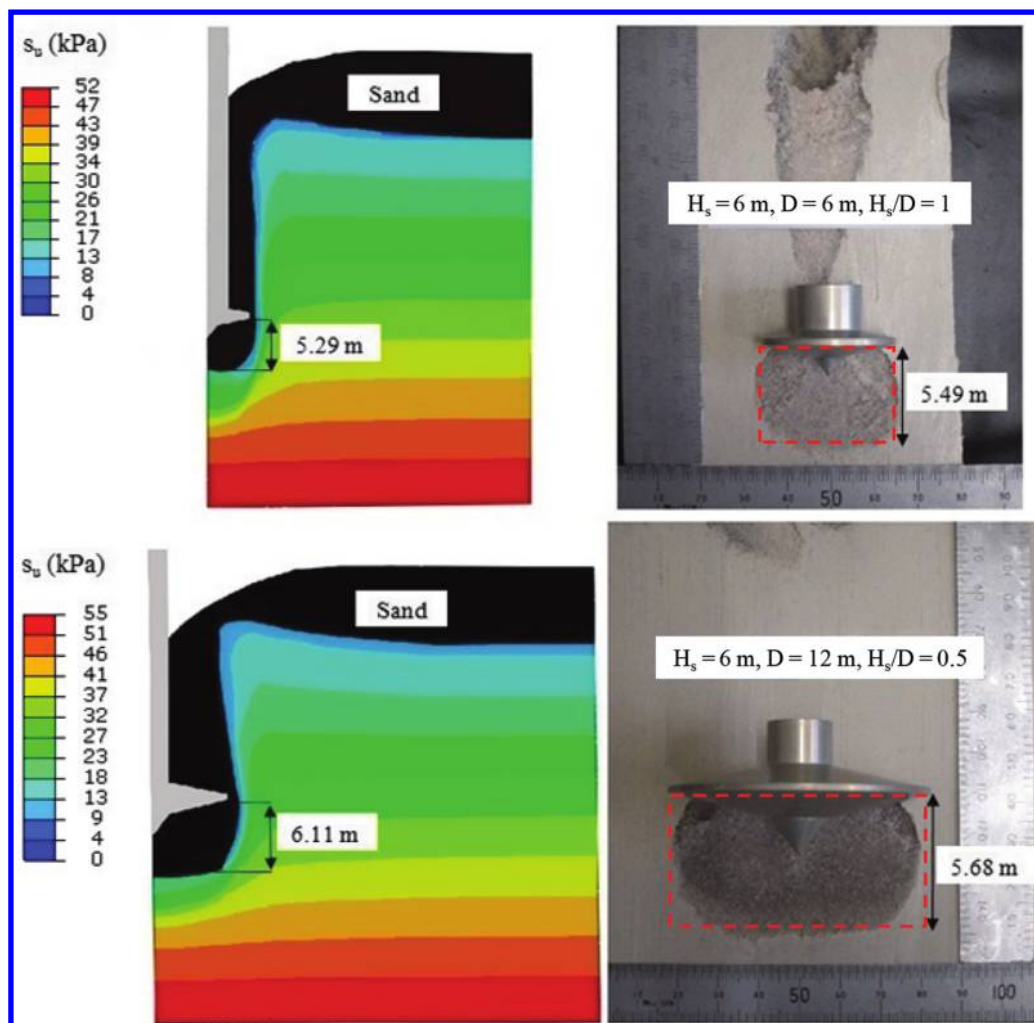
Fig. 12. (*a*) Comparison of calculated and experimental H_{plug} and (*b*) relationship between H_{plug} and H_s.
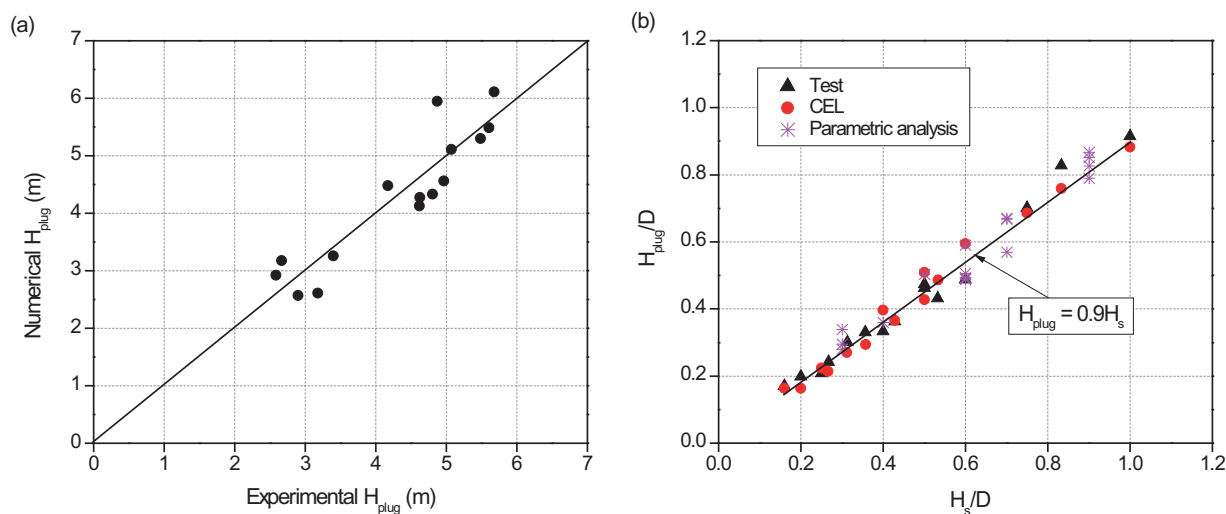
affected by the incomplete formation of the sand plug. Hence, for simplicity, N_c might be set equal to that estimated using eq. (8). For the majority of the analyses, the simple linear expression describes the bearing capacity factor with depth to within ±10% of the back-calculated values.

It should be noted that eq. (8) was summarized for $H_s/D = 0.16$–1, $\phi' = 30°$–$33°$, $s_{um} = 10$–40 kPa, $k = 1$–2 kPa/m, and sensitivity S_t in the range 3–5, all of which represent practical ranges of soil properties for offshore locations, where punch-through failure are potential risks. This equation may not be valid outside of these

Table 2. Summary of numerical parametric studies.

No. #	H_s (m)	D (m)	H_s/D	s_{um} (kPa)	k (kPa/m)	φ' (°)	H_{plug} (m)	$N_{c,\,deep}$
1	6	10	0.6	10	1	32	5.06	19.34
2	6	10	0.6	10	1.5	32	4.94	18.35
3	6	10	0.6	10	2	32	4.94	18.22
4	6	10	0.6	20	1	32	4.88	17.70
5	6	10	0.6	20	1.5	32	4.88	17.26
6	6	10	0.6	20	2	32	5.90	16.81
7	5.4	6	0.9	10	1.5	32	5.11	25.12
8	5.4	6	0.9	20	1.5	32	4.96	20.09
9	7	10	0.7	10	1.5	32	5.70	20.41
10	7	10	0.7	20	1.5	32	6.67	18.96
11	3	10	0.3	10	1.5	32	2.94	13.50
12	3	10	0.3	10	1.5	30	2.80	12.56
13	6	10	0.6	10	1.5	30	4.92	18.49
14	5.4	6	0.9	10	1.5	30	5.20	20.80
15	7	10	0.7	20	1.5	33	6.70	16.80
16	7	14	0.5	40	1.5	32	6.04	14.97
17	6.4	16	0.4	40	1.5	32	5.66	14.26
18	6	20	0.3	30	1.5	32	5.77	14.55

Fig. 13. Effects of H_s/D, k, and s_{um} on penetration resistance profiles: (*a*) effect of sand thickness ratio; (*b*) effect of clay strength.
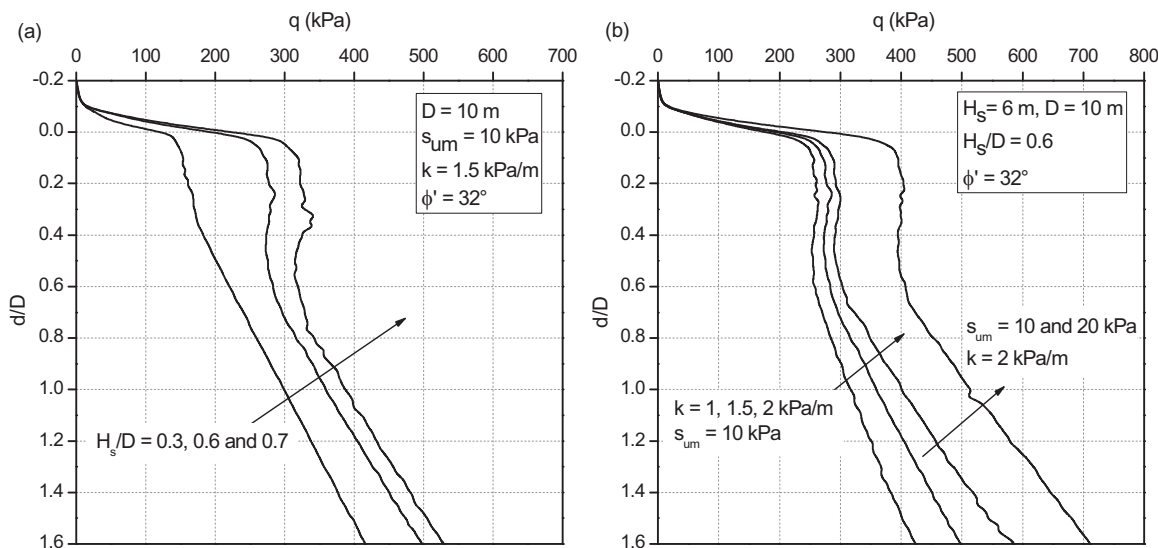
**Fig. 14.** Bearing capacity factors from CEL simulations of centrifuge tests and parametric studies.
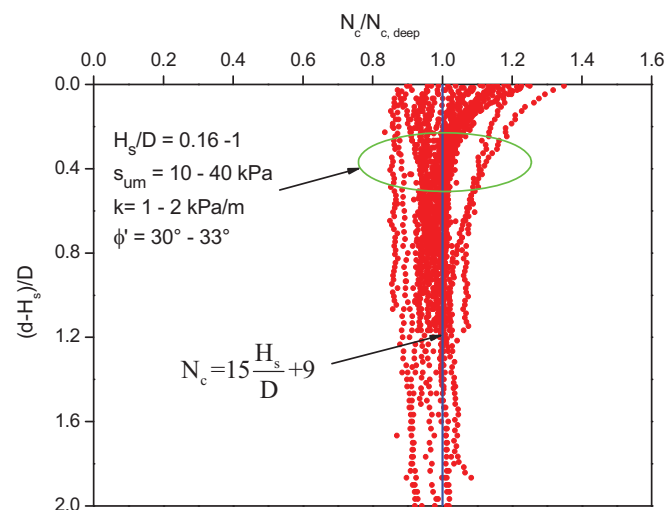
bounds or for soils with significantly differing behaviors (such as carbonate silts or highly sensitive clays).

Simplified method for prediction of full penetration resistance profile

A simplified full profile prediction method

A simplified method for the prediction of a penetration resistance profile for spudcan foundations on sand overlying clay is useful in the evaluation of the potential severity of a punch-through failure. The construction of a simplified resistance profile requires preliminary knowledge of three critical stages in $q{\sim}d$ space: (*i*) the penetration resistance from the tip of the spudcan touching the soil until the spudcan spigot (if present) is fully embedded, (*ii*) the peak resistance in the sand layer, q_{peak}, and (*iii*) the penetration resistance when the LRP is at the depth of the original sand–clay interface ($d = H_s$) and beyond. At stage (*i*), the resistance can be assumed to be zero for simplicity because the contribution of a small spigot to the overall capacity is negligible, and the corresponding penetration depth is the height of the spigot. At stage (*ii*), the modified failure stress dependent model of Hu et al. (2014) can be utilized

Fig. 15. Nomenclature of $d_{\text{punch, test}}$ and $d_{\text{punch, predicted}}$ for (a) medium dense and (b) dense sand tests.
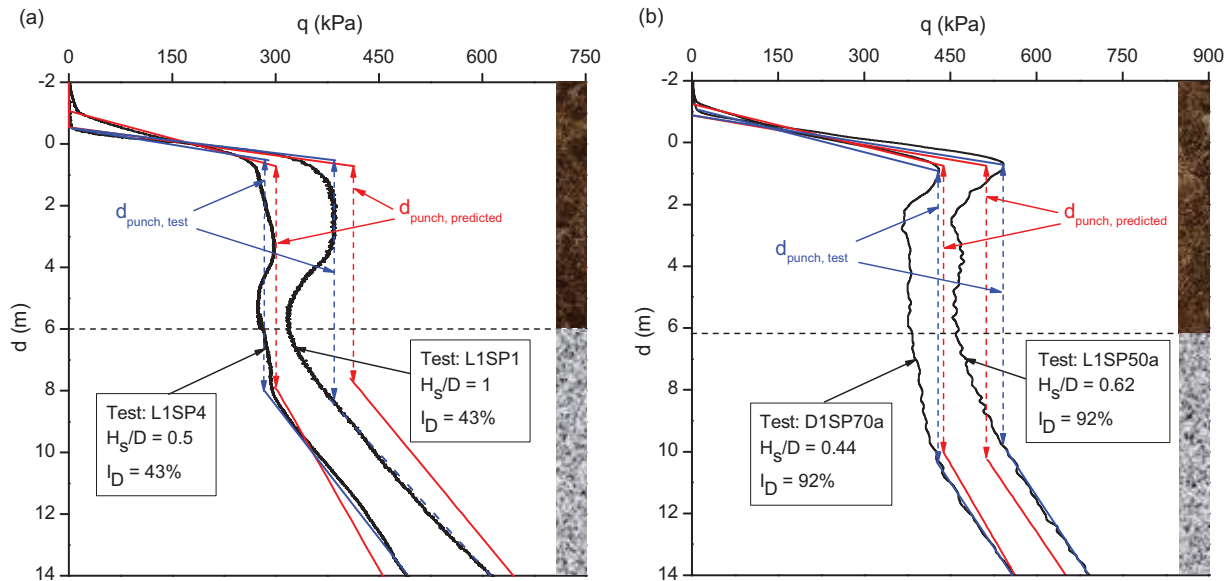
$$(9) \qquad q_{\text{peak}} = \left(N_{c0}s_{\text{um}} + q_0 + 0.12\gamma'_s H_S\right)\left(1 + \frac{1.76H_S}{D}\tan\psi\right)^{E^*}$$
$$+ \frac{\gamma'_s}{2\tan\psi(E^* + 1)}\left[1 - \left(1 - \frac{1.76H_S}{D}E^*\tan\psi\right)\right.$$
$$\left. \times \left(1 + \frac{1.76H_S}{D}\tan\psi\right)^{E^*}\right]$$

where N_{c0} is the bearing capacity factor for clay at the base of a circular foundation, which is obtained using the relationship proposed by Houlsby and Martin (2003) for circular foundations with shear strength increasing linearly with depth, and q_0 is the effective overburden pressure at the depth of the foundation. E^* is a parameter to simplify the algebra:

$$(10) \qquad E^* = 2\left[1 + D_F\left(\frac{\tan\phi^*}{\tan\psi} - 1\right)\right]$$

where D_F is a distribution factor that relates the local stress along the failure surface to the average vertical stress, or the ratio of the normal effective stress at the slip surface to the mean vertical effective stress, and ϕ^* is a reduced friction angle caused by non-associated flow that can be expressed as (Drescher and Detournay 1993):

$$(11) \qquad \tan\phi^* = \frac{\sin\phi'\cos\psi}{1 - \sin\phi'\sin\psi}$$

The depth of the peak penetration resistance, d_{peak}, is $0.12H_s$, as suggested by Teh et al. (2010) and verified through centrifuge tests for dense and medium dense sand overlying clay (Hu et al. 2014). For stage (iii) and beyond, the penetration resistance is calculated by substituting $N_{c,\text{deep}}$ in eq. (8) for N_c in eq. (7). The depth of the punch-through event is thus the depth at which the capacity by eq. (7) is equal to q_{peak} minus d_{peak}.

Performance of the simplified prediction method

To explore the performance of the proposed simplified prediction method, both the resistance profile and the depths of punch-through event were compared for 20 centrifuge tests of sand overlying clay in Table 1 (15 for medium dense sand overlying clay

from Hu et al. (2014) and 5 for dense sand overlying clay from Lee et al. (2013a)). Figure 15 demonstrates the comparisons for two pairs of typical tests from medium dense sand overlying clay and dense sand overlying clay. In general, the initial sharp increase in the resistance on sand and the resistance in the clay layer are predicted reasonably well for the four cases. This validates the model of Hu et al. (2014) for q_{peak} prediction and the equation proposed here for q_{clay} (eqs. (7) and (8)). If the depth of the peak resistance is also known, which has been demonstrated to be readily predicted (Hu et al. 2014: fig. 6 and eq. 3), the potential maximum depth of a punch-through event from onset until equilibrium is re-established can be estimated. It is acknowledged that for jack-up units that can perform preloading at draft this maximum distance may not be the primary concern, and the shape of the resistance profile after peak may be more critical. Though this is not provided in this simplified approach, the $d_{\text{punch, predicted}}$ value here gives an indication of severity. This figure also demonstrates that, even though it was derived from CEL simulations for loose and medium dense sand overlying clay, the simple prediction model for bearing capacity in the clay layer still appears valid for dense sand overlying clay scenarios. The soil at the periphery of the sand plug has reached the critical state during penetration in the clay layer — irrespective of the initial relative density of the sand layer — due to the cumulative shearing to which it is subjected. Hence, simulations setting the operative friction angle equal to the critical value also appear valid for dense sand overlying clay. It would be beneficial in the future to simulate the dense sand overlying clay centrifuge tests using a constitutive model for the sand that can account for strain hardening and softening.

The predictions of the simplified method for both medium dense and dense sand tests are also presented in terms of $d_{\text{punch, predicted}}/d_{\text{punch, test}}$ in Fig. 16. Though the predictions from the simplified method underestimate the uncontrolled penetration depth, the underprediction is less than 20% for the majority of the tests. Even with an underprediction of 20%, the method clearly allows a relatively fast and accurate prediction of the depth of a punch-through event that can be compared against the operability limits of the jack-up rig. All parameters are routinely derived during site investigation campaigns prior to jack-up rig deployment. It should be noted that the framework presented is verified by centrifuge tests of medium dense and dense sand overlying kaolin clay; more testing and field data with a wider range of material properties would further validate its performance.

Fig. 16. Performance of the simplified prediction method by comparison of rapid penetration depth with that obtained from centrifuge tests.
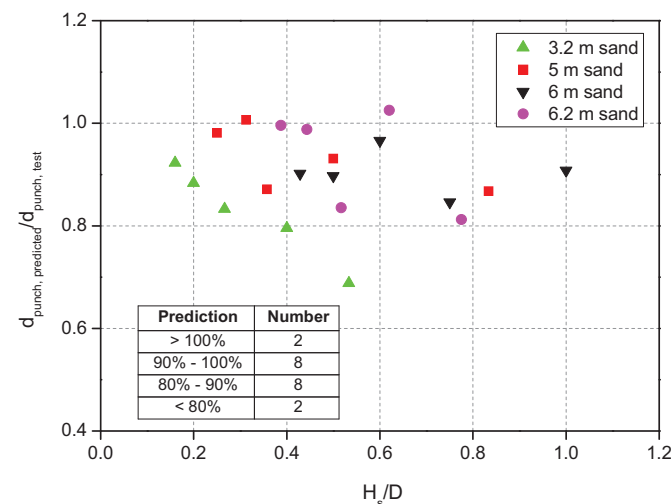
Conclusions

This paper reports the results of CEL simulations of centrifuge tests, investigating the potential for punch-through of spudcan foundations during deep penetration through a sand layer into an underlying clay layer. Generally reasonable agreement was obtained between the results of centrifuge tests and CEL analyses in terms of penetration resistance profiles. A simplified prediction method with straightforward algebraic expressions and clearly defined parameters for producing a complete simplified penetration resistance profile for foundations on sand overlying clay has been presented.

By incorporating strain softening clay constitutive model in the simulation, both punch-through and rapid-leg-run potential in medium dense sand overlying clay centrifuge tests were replicated. The contact property was shown to have only a small effect on q_{peak}, though more significant differences in q_{clay} were found for smooth and frictional cases in which the spudcan was fully embedded into the clay layer. The sensitivity of the clay, S_t, had a small effect on the penetration resistance when within the range of $3 \leq S_t \leq 5$.

Using complementary parametric analyses, the effects of H_s/D, k, and s_{um} on the penetration resistance profile were investigated. H_s/D mainly controls the pattern of failure potential, with larger values being more prone to punch-through failure (reduction of vertical load with depth), while rapid-leg-run (approximately constant peak load with depth) is more likely for smaller values of H_s/D. When H_s/D was further decreased, a nonlinear increase of the penetration resistance was apparent, indicating no punch-through or rapid-leg-run potential. The deep penetration resistance, q_{clay}, increased significantly with increasing s_{um}, while the gradient of q_{clay} was largely independent of s_{um} for clay with the same k. A linear expression for the bearing capacity factor for the spudcan and underlying plug is summarized from numerical simulations of centrifuge tests and complementary analyses. The equation is based on the geometric conditions and material properties relevant to spudcan punch-through and should be used with caution for any cases beyond the conditions explored in this manuscript (such as nonsiliceous sands or highly sensitive clays).

In the simplified prediction method, for penetration resistance in the upper sand layer, the stress level and dilatant response as well as the embedment depth are taken into account; for penetration in the underlying clay, the proposed design equations incorporate the shear strength increment with depth and the thickness of the trapped sand beneath the foundation. In retrospectively

calculating the penetration resistance profiles for all 15 medium dense sand and 5 dense sand centrifuge tests, the predicted full penetration resistance profiles show generally good agreement with the testing profiles. The simplified prediction method underpredicts the rapid penetration depth by less than 20%.

Acknowledgements

References

Andersen, K.H., and Jostad, H.P. 2004. Shear strength along inside of suction anchor skirt wall in clay. *In* Proceedings of the Offshore Technology Conference, Houston, Tex., 3–6 May 2004. OTC 16844.

Bolton, M.D. 1986. The strength and dilatancy of sands. Géotechnique, **36**(1): 65–78. doi:10.1680/geot.1986.36.1.65.

Cassidy, M.J. 2012. Experimental observations of the penetration of spudcan footings in silt. Géotechnique, **62**(8): 727–732. doi:10.1680/geot.9.T.020.

Cassidy, M.J., and Houlsby, G.T. 2002. Vertical bearing capacity factors for conical footings on sand. Géotechnique, **52**(9): 687–692. doi:10.1680/geot.2002.52.9.687.

Dassault Systèmes. 2011. ABAQUS analysis user's manual. Simulia Corp., Providence, R.I.

Drescher, A., and Detournay, E. 1993. Limit load in translational failure mechanisms for associative and non-associative materials. Géotechnique, **43**(3): 443–456. doi:10.1680/geot.1993.43.3.443.

Einav, I., and Randolph, M.F. 2005. Combining upper bound and strain path methods for evaluating penetration resistance. International Journal for Numerical Methods in Engineering, **63**(14): 1991–2016. doi:10.1002/nme.1350.

Finnie, I.M.S., and Randolph, M.F. 1994. Punch-through and liquefaction induced failure of shallow foundations on calcareous sediments. *In* Proceedings, International Conference on Behaviour of Offshore Structures, Boston. pp. 217–230.

Gan, C.T., Leung, C.F., Cassidy, M.J., Gaudin, C., and Chow, Y.K. 2012. Effect of time on spudcan-footprint interaction in clay. Géotechnique, **62**(5): 401–413. doi:10.1680/geot.10.P.063.

Hossain, M.S., and Randolph, M.F. 2009. Effect of strain rate and strain softening on the penetration resistance of spudcan foundations on clay. International Journal of Geomechanics, **9**(3): 122–132. doi:10.1061/(ASCE)1532-3641(2009)9:3(122).

Houlsby, G.T., and Martin, C.M. 2003. Undrained bearing capacity factors for conical footings on clay. Géotechnique, **53**(5): 513–520. doi:10.1680/geot.2003.53.5.513.

Hu, P., Stanier, S.A., Cassidy, M.J., and Wang, D. 2014. Predicting the peak resistance of spudcan penetrating sand overlying clay. Journal of Geotechnical and Geoenvironmental Engineering, **140**(2): 04013009. doi:10.1061/(ASCE)GT.1943-5606.0001016.

ISO. 2012. Petroleum and natural gas industries – site-specific assessment of mobile offshore units – part 1: jack-ups. International Organization for Standardization, ISO 19905-1.

Kvalstad, T.J., Nadim, F., and Harbitz, C.B. 2001. Deepwater geohazards: geotechnical concerns and solutions. *In* Proceedings of the Offshore Technology Conference, Houston. OTC 16844.

Lee, K.K. 2009. Investigation of potential spudcan punch-through failure on sand overlying clay soils. Ph.D. thesis, The University of Western Australia, Perth, Australia.

Lee, K.K., Cassidy, M.J., and Randolph, M.F. 2013*a*. Bearing capacity on sand overlying clay soils: Experimental and finite-element investigation of potential punch-through failure. Géotechnique, **63**(15): 1271–1284. doi:10.1680/geot.12.P.175.

Lee, K.K., Randolph, M.F., and Cassidy, M.J. 2013*b*. Bearing capacity on sand overlying clay soils: A simplified conceptual model. Géotechnique, **63**(15): 1285–1297. doi:10.1680/geot.12.P.176.

Li, X., Hu, Y., and White, D.J. 2013. Extension of Mohr–Coulomb model into state dependent softening of sand and its application in large deformation finite element analysis. *In* Proceedings of the 2nd International Symposium on Constitutive Modelling of Geomaterials: Advances and Applications, Beijing. Vol. 1, pp. 583–591.

Low, H.E., Randolph, M.F., DeJong, J.T., and Yafrate, N.J. 2008. Variable rate full-flow penetration tests in intact and remolded soil. *In* Proceedings of the

3rd International Conference on Geotechnical and Geophysical Site Characterization, Taylor and Francis, London. pp. 1087–1092.

Mehryar, Z., and Hu, Y. 2002. Penetration analysis of spudcan foundation in NC clay. *In* Proceedings of the 12th International Offshore and Polar Engineering Conference, Kitakyushu, Japan.

Osborne, J., Pelley, D., Nelson, C., and Hunt, R. 2006. Unpredicted jack-up foundation performance. *In* Proceedings of the 1st Jack-up Asia Conference, Singapore.

Qiu, G., and Grabe, J. 2012. Numerical investigation of bearing capacity due to spudcan penetration in sand overlying clay. Canadian Geotechnical Journal, **49**(12): 1393–1407. doi:10.1139/t2012-085.

Qiu, G., and Henke, S. 2011. Controlled installation of spudcan foundations on loose sand overlying weak clay. Marine Structures, **24**(4): 528–550. doi:10.1016/j.marstruc.2011.06.005.

Teh, K.L., Cassidy, M.J., Leung, C.F., Chow, Y.K., Randolph, M.F., and Quah, C.K. 2008. Revealing the bearing capacity mechanisms of a penetrating spudcan through sand overlaying clay. Géotechnique, **58**(10): 793–804. doi:10.1680/geot.2008.58.10.793.

Teh, K.L., Leung, C.F., Chow, Y.K., and Cassidy, M.J. 2010. Centrifuge model study

of spudcan penetration in sand overlying clay. Géotechnique, **60**(11): 825–842. doi:10.1680/geot.8.P.077.

Tho, K.K., Leung, C.F., Chow, Y.K., and Swaddiwudhipong, S. 2009. Application of Eulerian finite element technique for analysis of spudcan and pipeline penetration into the seabed. *In* Proceedings of the 12th International Jack-up Conference, London, 2009.

Tho, K.K., Leung, C.F., Chow, Y.K., and Swaddiwudhipong, S. 2012. Eulerian finite-element technique for analysis of jack-up spudcan penetration. International Journal of Geomechanics, **12**(1): 64–73. doi:10.1061/(ASCE)GM.1943-5622.0000111.

White, D.J., Teh, K.L., Leung, C.F., and Chow, Y.K. 2008. A comparison of the bearing capacity of flat and conical circular foundations on sand. Géotechnique, **58**(10): 781–792. doi:10.1680/geot.2008.3781.

Yu, L., Hu, Y., Liu, J., Randolph, M.F., and Kong, X. 2012. Numerical study of spudcan penetration in loose sand overlying clay. Computers and Geotechnics, **46**: 1–12. doi:10.1016/j.compgeo.2012.05.012.

Zhang, C., White, D., and Randolph, M. 2011. Centrifuge modeling of the cyclic lateral response of a rigid pile in soft clay. Journal of Geotechnical and Geoenvironmental Engineering, **137**(7): 717–729. doi:10.1061/(ASCE)GT.1943-5606.0000482.

This article has been cited by:

1. J. Zheng, M.S. Hossain, D. Wang. 2016. Prediction of spudcan penetration resistance profile in stiff-over-soft clays. *Canadian Geotechnical Journal* **53**:12, 1978-1990. [Abstract] [Full Text] [PDF] [PDF Plus]

2. Muhammad Shazzad Hossain, Stefanus Safinus, Mark J. Cassidy. 2015. Using a thin sand layer to ease spudcan extraction in clay. *Canadian Geotechnical Journal* **52**:8, 1023-1034. [Abstract] [Full Text] [PDF] [PDF Plus]